

Analysis of Multi-Frequency Oscillating Magnetic Fields by Neutron Spin Interferometry

Ryuto Fujitani^{1,2*}, Masahiro Hino², and Takashi Higuchi^{2,3}

¹Department of Nuclear Engineering, Kyoto University, Kyoto 615-8246, Japan

²Institute for Integrated Radiation and Nuclear Science (KURNS), Kyoto University, Kumatori, Osaka 590-0494, Japan

³Research Center for Nuclear Physics (RCNP), The University of Osaka, Osaka 567-0047, Japan

We have developed a methodology for analyzing multi-frequency oscillating magnetic fields using neutron spin interferometry. A theoretical formulation was derived of the contrast and the phase of the interference pattern for an input oscillating magnetic field consisting of a series of sine functions with multiple frequencies. According to the formulation, the contrast decays due to the dispersion of the Larmor precession induced by an oscillating field. The formulation also predicts that the phase of the interference pattern does not constant in contrast to single-frequency cases. We conducted an experiment in JRR-3 C3-1-2-2 beam port to confirm the formulation in the cases of two-frequency oscillating fields in the frequency range from 2500 Hz to 10000 Hz. The measured interference patterns showed reasonable agreement with the theoretical predictions.

1. Introduction

Neutrons are electrically neutral and have magnetic moments. This gives them both high penetration and sensitivity to magnetic fields, making them effective probes in materials science.¹⁻³⁾ Among methods employing neutrons, neutron spin interferometry (NSI) is one of the most sensitive methods for detecting magnetic fields, which relies on the detection of the Larmor precession phase between the two spin states as neutrons traverse a sample.³⁻¹⁴⁾ Techniques based on this principle, such as neutron spin echo (NSE), are widely used to study dynamics in soft matter, magnetic systems, and other media.¹⁵⁻¹⁷⁾

Neutrons are also useful for the magnetic field imaging due to high penetration ability. From the perspective of energy efficiency, the measurements of oscillating magnetic fields in materials, such as electric motors and transformers are becoming important. The use of stroboscopic systems for polarized neutron imaging of periodic, varying magnetic fields has also been studied.^{18,19)} However stroboscopic systems are limited by time scales. In previous work, we proposed a method to analyze single-frequency oscillating magnetic fields in the kilohertz range using neutron spin interferometry with continuous neutron exposure.²⁰⁾ In this study, we extend this approach to multi-frequency oscillating magnetic fields. We present the analytical formulation and demonstrate the validity of the proposed approach with experiments.

2. Neutron Spin Interferometry

In neutron spin interferometry, the spin states of polarized neutrons are manipulated by resonant spin flippers (RSFs) to create and control a superposition of their two spin states. When a neutron enters into an interferometer, it is polarized by a polarizer and transformed into a superposition state by a first RSF. The state of a neutron ψ after the first RSF can be written as

$$\psi = \frac{1}{\sqrt{2}} (|+\rangle - e^{i\chi_1} |-\rangle), \quad (1)$$

where $|+\rangle$ and $|-\rangle$ donate the spin-up and spin-down state, respectively, and χ_1 is the phase of the oscillating field generated by the first RSF. After passing through a magnetic field, a second RSF again generates a superposition of the spin states. Then, an analyzer polarizes a neutron:

$$\psi = \frac{1}{2} (e^{-i\phi} - e^{i(\phi - \chi_2 + \chi_1)}) |+\rangle, \quad (2)$$

where χ_2 is the phase of the oscillating field generated by the second RSF, and ϕ is the phase induce by the magnetic field between two RSFs. Note that a neutron experiences a potential of the opposite sign depending on its spin state. Consequently, the magnetic field generates a phase between the two spin states. By defining $\chi = \chi_2 - \chi_1$, the detection probability of a neutron is given by

$$|\psi|^2 = \frac{1}{2} \{1 - \cos(\chi - 2\phi)\}. \quad (3)$$

Thus, a sinusoidal interference pattern can be obtained. The experimentally observed interference pattern is shown in Fig.3.

In experimental measurements, this pattern is observed as the neutron count N , which can be expressed as follows:

$$N = \frac{N_0}{2} \{1 - \cos(\chi - \Omega - \delta)\}, \quad (4)$$

where N_0 is neutron counts without RSFs. The terms δ and Ω represent the phases induced by the guide magnetic field and the magnetic field between RSFs, respectively. These phases satisfy $2\phi = \delta + \Omega$. Since a guide magnetic field is applied throughout the neutron spin interferometer system to maintain spin orientation, a consistent phase exists across measurements. To distinguish the guide field contribution, the constant phase offset δ is introduced. The phase shift Ω is expressed by the following integral of the magnetic field between RSFs:

$$\Omega = \frac{2|\mu_n|}{\hbar v} \int_0^l B(x) dx, \quad (5)$$

where \hbar is the Dirac's constant, μ_n is the magnetic moment of the neutron, v is the neutron velocity, and l is the distance

*fujitani.ryuto.85m@st.kyoto-u.ac.jp

between RSFs. $B(x)$ is the strength of the magnetic field along the neutron path x between the RSFs.

In practice, due to a finite polarization efficiencies of the polarizer and the analyzer, as well as the spin-flip efficiency of RSFs, the contrast of an interference pattern C does not reach unity. Therefore, the experimentally observed interference pattern is described by

$$N = \frac{N_0}{2} \{1 - C \cos(\chi - P)\}, \quad (6)$$

where the phase of an interference pattern is P . Parameters C , P and N_0 can be extracted by fitting to Eq.(6).

3. Theoretical Description

3.1 Formulation of a Multi-Frequency Oscillating Magnetic Field

A multi-frequency oscillating magnetic field $B(x, t)$ at position x and time t can be expressed as a Fourier series expansion based on the fundamental frequency f .

$$B(x, t) = B_0(x) \sum_{n=1}^{\infty} d_n \sin(-2\pi nft + \phi_n) \quad (7)$$

Here, ϕ_n denotes the phase of the n -th frequency component oscillation, and d_n is the amplitude of the n -th component normalized by the fundamental amplitude ($d_1 = 1$). $B_0(x)$ represents the strength of the magnetic field without time dependency.

When a neutron enters a region of an oscillating magnetic field at time τ , in the same way as in Eq. (5), the phase shift Ω observed in spin interference is given by

$$\Omega(\tau) = \frac{2|\mu_n|}{\hbar v} \int_0^l B_0(x) \sum_{n=1}^{\infty} d_n \sin(-2\pi fn(t - \tau) + \phi_n) dx. \quad (8)$$

Since the magnetic field oscillates while a neutron traverses the field, the magnetic field experienced by a neutron is obtained by substituting $t = x/v$ into Eq. (8). Thus, Eq. (8) can be rewritten as

$$\Omega(\theta) = \frac{2|\mu_n|}{\hbar v} \int_{-\infty}^{\infty} B_0(x) \sum_{n=1}^{\infty} d_n \sin\left(-\frac{2\pi f}{v} nx + n\theta + \phi_n\right) dx. \quad (9)$$

Here, θ represents the phase of the oscillating magnetic field at the moment a neutron enters the field, defined by $\theta = 2\pi f\tau$. By assuming $B_0(x) = 0$ at $x \leq 0$ or $x \geq l$, the integration range has been extended to infinity. Eq. (9) provides the expression of Ω for an oscillating magnetic field, corresponding to the static case in Eq. (5). Introducing

$$k = 2\pi f/v, \quad (10)$$

and using the k -space Fourier transform of the magnetic field profile $B_0(x)$, the power spectrum $|b(k)|$ and the phase $\theta(k)$ are defined as

$$|b(k)|e^{i\theta(k)} = \int_{-\infty}^{\infty} B_0(x)e^{-ikx} dx. \quad (11)$$

Extracting only the imaginary part of Eq. (11) gives

$$|b(k)| \sin(\theta(k)) = \int_{-\infty}^{\infty} B_0(x) \sin(-kx) dx. \quad (12)$$

Thus, the phase shift $\Omega(\theta)$ can be rewritten as

$$\Omega(\theta) = \frac{2|\mu_n|}{\hbar v} \sum_{n=1}^{\infty} |b(nk)|d_n \sin(n\theta + \phi_n + \theta(nk)). \quad (13)$$

3.2 Formulation of an Interference Pattern

Consider an interference pattern obtained for an oscillating magnetic field with continuous exposure. In the case of continuous exposure, the phase θ can take any value within the range $0 \leq \theta \leq 2\pi$. Therefore, the observed interference pattern corresponds to an average over all the values of θ . Consequently, an observed interference pattern is given by

$$N = \frac{N_0}{2} \frac{1}{2\pi} \int_0^{2\pi} \{1 - \cos(\chi - \Omega(\theta) - \delta)\} d\theta. \quad (14)$$

This equation describes an integration of the dispersion of the phase shift. Introducing the complex value c defined as

$$c = \frac{1}{2\pi} \int_0^{2\pi} \exp(i\Omega(\theta))d\theta, \quad (15)$$

an interference pattern can be written as

$$N = \frac{N_0}{2} \{1 - |c| \cos(\chi - \delta - \arg(c))\}. \quad (16)$$

The value of c will be

$$c = \sum_{\substack{m_1+2m_2+3m_3+\dots=0 \\ m_k \in \mathbb{Z}}} J_{m_1} \left(\frac{2|\mu_n|}{\hbar v} |b(k)| \right) J_{m_2} \left(\frac{2|\mu_n|}{\hbar v} |b(2k)|d_2 \right) \dots \\ \times \exp\{i(m_1(\phi_1 + \theta(k)) + m_2(\phi_2 + \theta(2k)) + \dots)\}, \quad (17)$$

where \mathbb{Z} denotes the set of all integers and $J_m(x)$ denotes the m -th order Bessel function of the first kind.

The derivation of Eq. (17) is as follows. We use the generating function of the Bessel function, given by

$$\exp\left(\frac{u}{2} \left(w - \frac{1}{w}\right)\right) = \sum_{m=-\infty}^{\infty} J_m(u)w^m, \quad (18)$$

where w and u are arbitrary complex numbers, with $w \neq 0$. By multiplying both sides, we obtain

$$\prod_{n=1}^{\infty} \exp\left(\frac{u_n}{2} \left(w_n - \frac{1}{w_n}\right)\right) = \prod_{n=1}^{\infty} \sum_{m_n=-\infty}^{\infty} J_{m_n}(u_n)w_n^{m_n}. \quad (19)$$

Setting $w_n = e^{i(n\theta + \phi_n + \theta(nk))}$ and $u_n = \frac{2|\mu_n|}{\hbar v} |b(nk)|d_n$, the left hand side of Eq. (19) becomes

$$\exp\left(i \sum_{n=1}^{\infty} \frac{2|\mu_n|}{\hbar v} |b(nk)|d_n \sin(n\theta + \phi_n + \theta(nk))\right) = \exp(i\Omega(\theta)) \quad (20)$$

while the right hand side of Eq. (19) becomes

$$\prod_{n=1}^{\infty} \sum_{m_n=-\infty}^{\infty} J_{m_n} \left(\frac{2|\mu_n|}{\hbar v} |b(nk)|d_n \right) \exp(im_n(n\theta + \phi_n + \theta(nk))). \quad (21)$$

Integrating both sides with respect to θ from 0 to 2π , and making use of the orthogonality in θ , we obtain Eq. (17).

3.3 Case of a Single-Frequency Oscillation

Consider the case in which a single-frequency oscillation is applied. Under this condition, $d_n = 0$ for $n \geq 2$. Using the properties of the Bessel function, $J_0(0) = 1$ and $J_n(0) = 0$ for

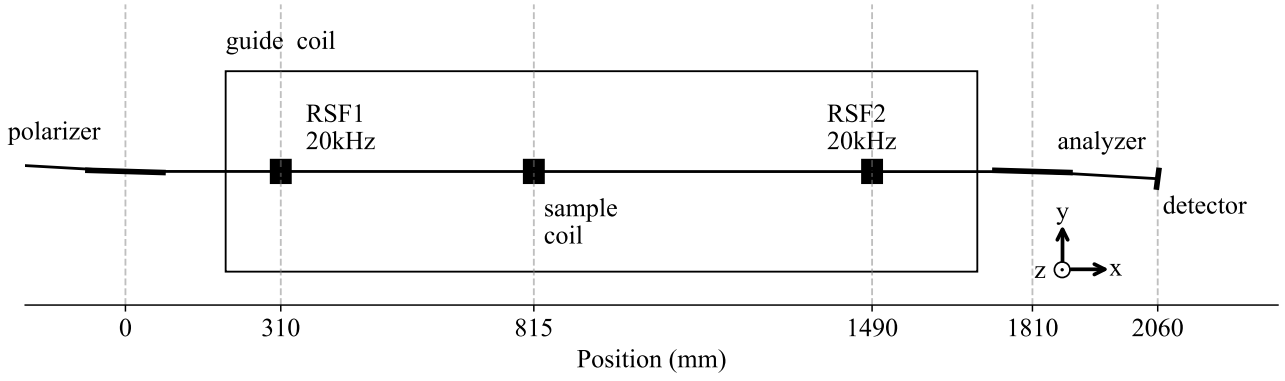


Fig. 1. Experimental setup for a neutron spin interferometer at JRR-3 C3-1-2-2.

$n \neq 0$, Eq.(17) becomes

$$c = J_0 \left(\frac{2|\mu_n|}{\hbar v} |b(k)| \right). \quad (22)$$

This result corresponds to the expression previously reported.²⁰⁾ Since c is always real and $\arg(c)$ shown in Eq. (16) is always zero, the phase of an interference pattern remains constant, while only the contrast decays following the zero-th order Bessel function.

3.4 Case of a Fundamental and Second-Harmonic Oscillations

Consider a fundamental and second-harmonic oscillations, given by

$$B(x, t) = B_0(x) \{ \sin(-2\pi ft + \phi_1) + d_2 \sin(-4\pi ft + \phi_2) \}. \quad (23)$$

Introducing $d_n = 0$ for $n \geq 3$, Eq.(17) becomes

$$c = \sum_{m=-\infty}^{\infty} J_{-2m} \left(\frac{2|\mu_n|}{\hbar v} |b(k)| \right) J_m \left(\frac{2|\mu_n|}{\hbar v} |b(2k)| d_2 \right) \times \exp \{ i(-2m(\phi_1 + \theta(k)) + m(\phi_2 + \theta(2k))) \}. \quad (24)$$

Since c can be a complex value and $\arg(c)$ shown in Eq. (16) is not always zero, the phase of an interference pattern can be shifted due to the oscillating magnetic field.

4. Experimental setup

To demonstrate Eq. (22) and Eq. (24), we conducted an experiment at JRR-3 C3-1-2-2 (Multilayer Interferometer and reflectometer for NEutron 2, MINE2). The incident neutron beam is continuous and monochromated to a wavelength of 8.8 Å and FWHM of the distribution is 2.7%.

The experimental setup is shown in Fig. 1. The beam direction is along the x -axis. The setup of a spin interferometer consists, in order from the upstream, of polarizer, RSF1, sample coil, RSF2, analyzer, and neutron detector. A guide magnetic field is applied throughout the entire spin interferometer system to maintain the neutron spin quantization axis.

The polarizer and analyzer, which reflect only spin-up neutrons, are composed of magnetic multilayer mirrors. The RSFs, which flip the neutrons spin direction, generate 20 kHz oscillating magnetic fields along the x -axis. The oscillating magnetic field to be analyzed by the spin interferometry is produced by a rectangle coil named sample coil. Its dimen-

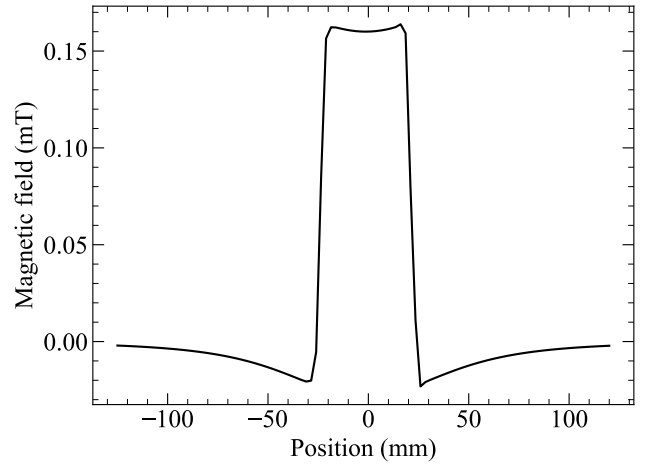


Fig. 2. A magnetic field generated by sample coil when 1 A current is applied. The calculation is performed based on the Biot-Savart law.

sions are 100 mm in the z -direction (height), 45 mm in the x -direction (length), and 70 mm in the y -direction (width) and consists of 15 turns. Its wire has 1 mm thickness and is made of Al, enabling lower neutron absorption. The spatial distribution of the magnetic field for 1 A current at the center of the coil along the x -axis shown in Fig. 2. This is the result of a calculation based on the Biot-Savart law.

An interference pattern obtained with this setup is shown in Fig. 3. Fitting the data to Eq. (6), the contrast C of the interference pattern is determined to be 0.9659 ± 0.0077 and the phase P is 33.65 ± 0.64 deg.

To demonstrate Eq. (22), We applied a single-frequency oscillating current to the coil. Interference patterns were measured while varying the amplitude of the AC current from 0.0 to 3.0 App. Measurements were carried out at frequencies from 2500 to 20000 Hz.

Subsequently, to demonstrate Eq. (24), we applied an AC current composed of a fundamental and second-harmonic oscillations. We measured interference patterns while varying the phase ϕ_2 of a double frequency oscillation shown in Eq. (24) from 0 deg to 360 deg. The amplitude of AC current for a fundamental oscillation was fixed to 2 App, while the relative amplitude of a second-harmonic oscillation, de-

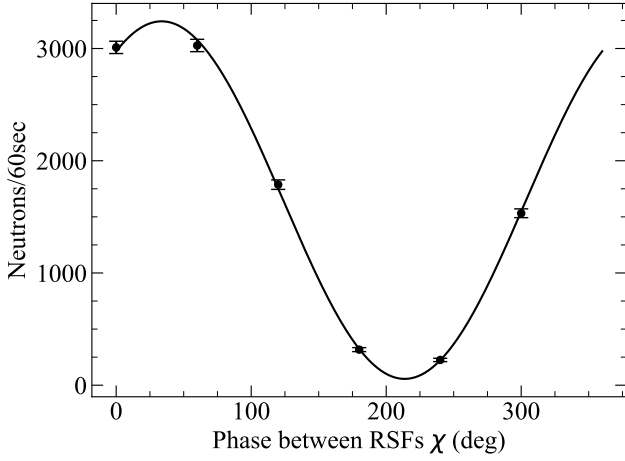


Fig. 3. An interference pattern obtained from a spin interferometer shown in Fig.1

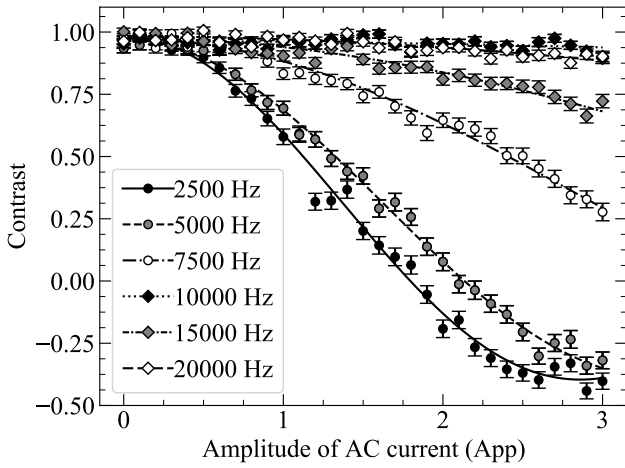


Fig. 4. The contrast of interference patterns varying with the amplitude of the sinusoidal AC current applied to the coil.

noted as d_2 , was varied among 0.25, 0.5, 0.75 and 1. Measurements were performed for fundamental frequencies from 2500, 5000, 7500 and 10000 Hz.

5. Results and Discussion

5.1 Case of a Single-Frequency Oscillation

The vertical axis in Fig. 4 represents the contrast of the interference pattern, while the horizontal axis indicates the amplitude of the AC current applied to the coil. Data for each frequency are plotted on the same graph. The plots represent experimental data, which have been scaled by a factor of $1/0.9659$, the inverse of the contrast observed without the sample, as shown in Fig. 3. The lines represent fits to the zero-th order Bessel function $J_0(x)$. As given in Eq. (24), the contrast follows the zero-th order Bessel function. By defining the $|b_{1App}(k)|$ which is $|b(k)|$ value when 1App current is applied, the contrast as a function of the AC current amplitude I can be fitted by

$$J_0\left(\frac{2|\mu_n|}{\hbar v}|b_{1App}(k)| \times I\right). \quad (25)$$

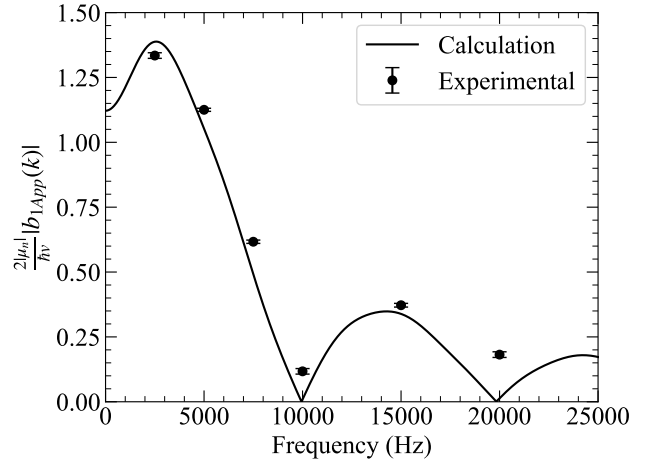


Fig. 5. Comparison of the calculated and measured values of $2|\mu_n||b_{1App}(k)|/\hbar v$. The calculated values are obtained from $B(k)$ shown in Fig. 2 using the Biot–Savart law and a neutron velocity corresponding to 8.8Å. These are compared with the measured values shown in Fig. 4.

From this fitting, the value of $2|\mu_n||b_{1App}(k)|/\hbar v$ can be extracted.

Fig. 5 shows the values of $2|\mu_n||b_{1App}(k)|/\hbar v$ as a function of frequency of the oscillating magnetic field. The line represents the value calculated using the magnetic field shown in Fig. 2. The plots are obtained from the measured results shown in Fig. 4. Since k is proportional to the frequency, the values of $2|\mu_n||b_{1App}(k)|/\hbar v$ have a frequency dependence.

The experimental data reproduce the estimation well. The remaining discrepancy can be considered to be imperfections in the coil shape. While the calculated values were obtained using the Biot–Savart law, distortions in the coil or its installation angle can affect the value of $|b_{1App}(k)|$.

5.2 Case of a Fundamental and a Second-Harmonic Oscillation

The contrast measured as a function of the phase of a second harmonic oscillation ϕ_2 is shown in Fig. 6, and the phase is shown in Fig. 7. These results correspond to the case where the fundamental oscillation of the applied current is 2 App. Here, the frequency refers to that of a fundamental oscillation. The contrast is scaled by a factor of $1/0.9659$. The lines represent calculated results based on Eq. (24) and measured $2|\mu_n||b_{1App}(k)|/\hbar v$ in Fig. 5. In the calculation, the summation was performed over the range $m = -20 \sim 20$.

In the experiments, the AC current was generated by function generator and power amplifier. Due to the inductance, determining the phase of a second harmonic oscillation ϕ_2 is difficult. Therefore, in Fig. 6 and Fig. 7, the experimental plot is shifted horizontally to the calculation results with the phases ϕ_2 .

Both the contrast and phase exhibit periodic behavior with respect to ϕ_2 , but they are not analytically simple such as sinusoidal. Despite the complexity of these variations, the experimental results show reasonable reproducibility.

For data with the fundamental frequency of 2500 Hz, the contrast and phase shown in Fig. 6 and Fig. 7 exhibit the most significant changes among four frequencies. Changes in the phase of second-harmonic oscillation depend on the

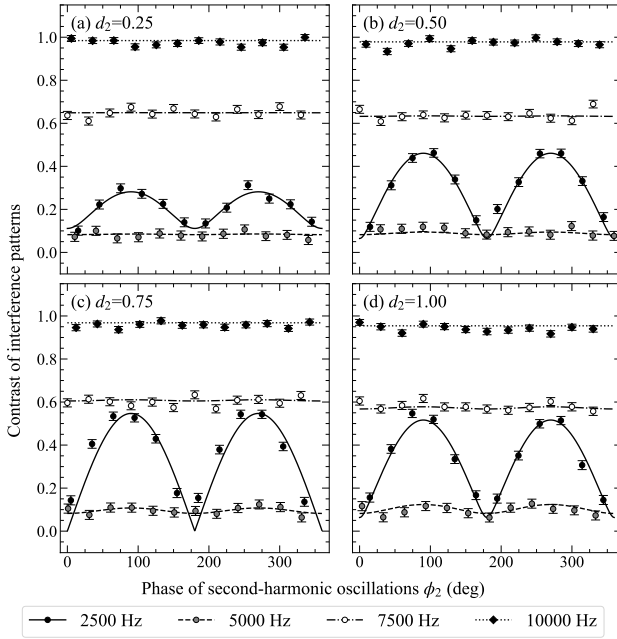


Fig. 6. The contrast of interference patterns when an amplitude of a fundamental oscillation is $2A_{pp}$ (a) the value of $d_2 = 0.25$ (b) the value of $d_2 = 0.50$ (c) the value of $d_2 = 0.75$ (d) the value of $d_2 = 1$. To calculate the estimation lines, measured $2|\mu_n||b_{1A_{pp}}(k)|/\hbar v$ values shown in Fig. 5 are used.

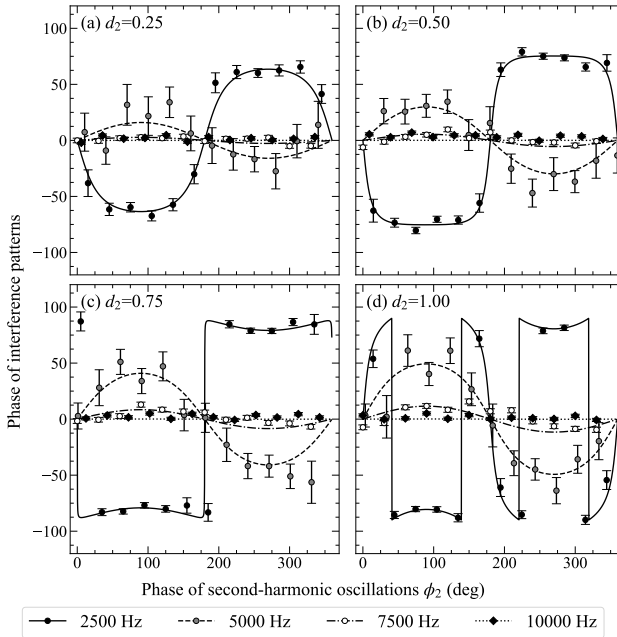


Fig. 7. The phase of interference patterns when an amplitude of a fundamental oscillation is $2A_{pp}$ (a) the value of $d_2 = 0.25$ (b) the value of $d_2 = 0.50$ (c) the value of $d_2 = 0.75$ (d) the value of $d_2 = 1$. To calculate the estimation lines, measured $2|\mu_n||b_{1A_{pp}}(k)|/\hbar v$ values shown in Fig. 5 are used.

value of $2|\mu_n||b_{1A_{pp}}(2k)|/\hbar v$ for the corresponding second-harmonic. As shown in Fig. 5, the value $2|\mu_n||b_{1A_{pp}}(k)|/\hbar v$ of 5000 Hz has the highest value among 5000, 10000, 15000 and 20000 Hz, which are the second-harmonic frequencies of 2500, 5000, 7500 and 10000 Hz. Consequently, the data for 2500 Hz show the most significant changes. In contrast, the

value $2|\mu_n||b_{1A_{pp}}(k)|/\hbar v$ has smaller values at 10000, 15000 and 20000 Hz. Therefore, the data with fundamental frequencies are 5000, 7500 and 10000 Hz show slight changes in contrast and phase.

To evaluate the effective frequency range, we consider a rectangular magnetic field $B_0(x)$ whose length is L , frequency is f and the strength is B :

$$B_0(x) = \begin{cases} B & 0 \leq x \leq L \\ 0 & \text{otherwise.} \end{cases} \quad (26)$$

From Eq. (11), the following equation can be obtained:

$$\frac{2|\mu_n|}{\hbar v}|b(k)| = \frac{2|\mu_n|}{\hbar} \frac{B}{\pi f L} \left| \sin\left(\frac{\pi f L}{v}\right) \right|. \quad (27)$$

Eq. (27) shows that $2|\mu_n||b(2k)|/\hbar v$ vanishes at $fL/v = 1$ and generally decreases as f increases. Thus, the fundamental frequency f should satisfy $f < v/L$ in order to obtain measurable changes. The n -th harmonics remains also observable as long as $nf < v/L$. Although the magnetic field in this experiment is not perfectly rectangular as shown in Fig. 2, a rough estimation is sufficient for this study. Given the conditions of $L = 45$ mm and $v = 450$ m/s, $2|\mu_n||b(k)|/\hbar v$ becomes zero at $f = 10000$ Hz and smaller for $f > 10000$ Hz. Therefore, the data in Fig. 6 and Fig. 7, which have fundamental frequencies of 5000 Hz, 7500 Hz and 10000 Hz, have small variations. Notably, at 10000 Hz, the contrast remains almost unity.

6. Conclusion

We presented the approach for analyzing multi-frequency sinusoidal oscillating magnetic fields in neutron spin interferometry. We derived a formulation of the resulting interference patterns assuming the oscillating field as a multi-frequency oscillation represented as a Fourier series expansion. The contrast and phase of the interference pattern were expressed as sums of sine functions weighted by Bessel functions. This was confirmed by an experiment with an oscillating magnetic field composed of a fundamental and second-harmonic oscillation in a frequency range from 2500 Hz to 10000 Hz. Although the resulting interference patterns are not analytically simple, the experimental data showed reasonable agreement with theoretical predictions, demonstrating the validity of the proposed approach.

Acknowledgment

This neutron experiment at JRR-3 C3-1-2-2 was carried out by the JRR-3 general user program managed by the Institute for Solid State Physics, the University of Tokyo (proposal No. 24583, 24407). The polarizing devices fabrication work has been conducted under the visiting researcher's program of the Institute for Integrated Radiation and Nuclear Science, Kyoto University. The development of neutron mirrors was also supported by the visiting Researcher's Program of the Research Reactor Institute, Kyoto University and JSPS KAKENHI (Grant No. 23K23274). This work is also financially supported by JST FOREST Program (Grant No. JP-MJFR2237).

1) H. Börner, J. Brown, C. Carlile, R. Cubitt, R. Currat, A. Dianoux, B. Farago, A. Hewat, J. Kulda, E. Lelièvre-Berna, et al.: ILL: Grenoble,

- France (2003).
- 2) N. Kardjilov, I. Manke, A. Hilger, M. Strobl, and J. Banhart: *Materials Today* **14** (2011) 248.
 - 3) M. Utsuro and V. K. Ignatovich: *Handbook of neutron optics* (John Wiley & Sons, 2010).
 - 4) V. Baryshevskii, S. Cherepitsa, and A. Frank: *Physics Letters A* **153** (1991) 299.
 - 5) G. Badurek, H. Rauch, and D. Tuppinger: *Physical Review A* **34** (1986) 2600.
 - 6) A. Frank, I. Bondarenko, A. Kozlov, G. Ehlers, and P. Høghøj, *Neutron Spin Precession Optics: Recent Results and Some Perspectives, Neutron Spin Echo Spectroscopy: Basics, Trends and Applications*, pp. 165–175. Springer, 2002.
 - 7) D. Yamazaki: *Nuclear Instruments and Methods in Physics Research Section A: Accelerators, Spectrometers, Detectors and Associated Equipment* **488** (2002) 623.
 - 8) M. Hino, N. Achiwa, S. Tasaki, T. Ebisawa, T. Kawai, and D. Yamazaki: *Phys. Rev. A* **61** (1999) 013607.
 - 9) M. Hino, N. Achiwa, S. Tasaki, T. Ebisawa, T. Kawai, T. Akiyoshi, and D. Yamazaki: *Phys. Rev. A* **59** (1999) 2261.
 - 10) N. Achiwa, T. Ebisawa, M. Hino, D. Yamazaki, G. Shirozu, S. Tasaki, and T. Kawai: *Physica B: Condensed Matter* **311** (2002) 61.
 - 11) M. Utsuro: *Physica B: Condensed Matter* **358** (2005) 232.
 - 12) Y. Hasegawa, R. Loidl, G. Badurek, M. Baron, and H. Rauch: *Nature* **425** (2003) 45.
 - 13) H. Bartosik, J. Klepp, C. Schmitzer, S. Sponar, A. Cabello, H. Rauch, and Y. Hasegawa: *Physical review letters* **103** (2009) 040403.
 - 14) J. Shen, S. J. Kuhn, R. M. Dalgliesh, V. de Haan, N. Geerits, A. A. Irfan, F. Li, S. Lu, S. R. Parnell, J. Plomp, et al.: *Nature communications* **11** (2020) 930.
 - 15) F. Mezei, C. Pappas, and T. Gutberlet: *Neutron spin echo spectroscopy: Basics, trends and applications* (Springer Science & Business Media, 2002), Vol. 601.
 - 16) R. Golub and R. Gähler: *physics letters A* **123** (1987) 43.
 - 17) R. Gähler, R. Golub, and T. Keller: *Physica B: Condensed Matter* **180** (1992) 899.
 - 18) A. S. Tremsin, N. Kardjilov, M. Strobl, I. Manke, M. Dawson, J. B. McPhate, J. V. Vallerga, O. H. W. Siegmund, and W. B. Feller: *New Journal of Physics* **17** (2015) 043047.
 - 19) *Development of AC Magnetic Field Imaging Technique Using Polarized Pulsed Neutrons at J-PARC* ().
 - 20) T. Suzuki, R. Fujitani, S. Tasaki, M. Hino, M. Kitaguchi, T. Oda, and R. Nakamura: *Journal of the Physical Society of Japan* **93** (2024) 091008.